

# Interaction of sine-Gordon kinks with defects: The two-bounce resonance

Roy H. Goodman\* Richard Haberman†

October 21, 2018

## Abstract

A model of soliton-defect interactions in the sine-Gordon equations is studied using singular perturbation theory. Melnikov theory is used to derive a critical velocity for strong interactions, which is shown to be exponentially small for weak defects. Matched asymptotic expansions for nearly heteroclinic orbits are constructed for the initial value problem, which are then used to derive analytical formulas for the locations of the well known two- and three-bounce resonance windows, as well as several other phenomena seen in numerical simulations.

## 1 The two-bounce resonance

The two-bounce resonance is a phenomenon displayed by many non-integrable systems in which a solitary wave interacts either with another solitary wave or else with a localized defect in the medium through which it propagates. Fei, Kivshar, and Vázquez study the two-bounce resonance in the sine-Gordon equation perturbed by a localized nonlinear defect [8].

$$u_{tt} - u_{xx} + \sin u = \epsilon \delta(x) \sin u. \quad (1.1)$$

Kink solitons are initialized propagating (numerically) toward a defect with velocity  $v_i$  and allowed to interact with the defect. Then one of two things might happen: either the soliton is trapped and comes to rest at the defect location, or else it escapes and propagates away at finite speed  $v_f$ . (The soliton cannot be destroyed by the interaction because it is defined by its boundary conditions at infinity.) They find that there exists a critical velocity  $v_c$ . Kink solitons with initial velocity greater than  $v_c$  pass by the defect. Most solitons with initial speeds below the  $v_c$  are trapped, remaining at the defect for all times after the interaction time. However, there exist bands of initial velocities, known

---

\*Department of Mathematical Sciences, New Jersey Institute of Technology, Newark, NJ 07102

†Department of Mathematics, Southern Methodist University, Dallas, TX 75275

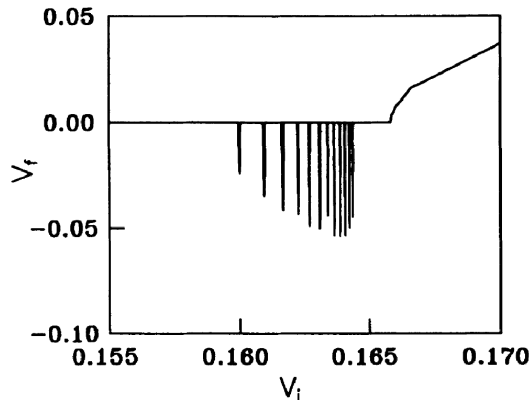


Figure 1.1: The output vs. input velocities of sine-Gordon solitons interacting with a delta-well defect, from [8], reprinted with permission.

as resonance windows, for which the kink is reflected by the defect, rather than being trapped. This is summarized in Figure 1.1, taken from their paper.

A phenomenological explanation for this phenomenon (in the context of kink-antikink interactions in nonlinear Klein-Gordon equations) was given by Campbell et. al. [4, 19, 3, 2] in a series of papers. They use very elegant physical reasoning to argue that the resonance windows are due to a resonant interaction between the movement of the kink-antikink pair in an effective potential, and shape modes oscillating about the kinks. Fei et. al. give an analysis of the two-bounce resonance phenomenon which relies on a variational approximation, which reduces the sine-Gordon PDE to a pair of second order ODE, and use a similar argument to find the resonance windows. Both these studies make the assumptions that the resonance takes a certain form, dependent on unknown constants, and use a mix of physical reasoning and statistical data fitting to find these constants.

An inspiration for the present work comes from one of the authors' previous studies of the trapping of gap solitons in Bragg grating optical fibers with defects [10]. In that study, sufficiently slow solitons in certain parameter regimes were captured by localized defects. This previous work does not offer a mechanism to explain the existence of a critical velocity for soliton capture, which we are now able to explain for the simpler model problem discussed here. The two bounce resonance phenomenon is also seen by Tan and Yang in simulations of vector solitons collisions in birefringent optical fibers [21].

The aim of the current paper is to make mathematically precise the physical reasoning of the previous studies of the two-bounce resonance, in a way that does not rely on statistical inference. We analyze the variational ODE model derived in [8]. We use the methods of singular perturbation theory to match a

nonlinear saddle to nearly heteroclinic orbits in a manner similar to that previously used by Haberman [12, 13] and Diminnie and Haberman [6, 7]. The critical velocity is determined via a Melnikov integral and the location of the resonance windows arises naturally due to a matching condition in the expansion. Intriguingly, finding the critical velocity requires that we make use of terms which are small beyond all orders in  $\epsilon$  in the matched asymptotic expansion, as was done, notably, by Kruskal and Segur [15], and by many others.

Other work on soliton dynamics in perturbed sine-Gordon equations is summarized by Scott [20]. In this approach, an ordinary differential equation is derived for the evolution of the Hamiltonian, which can then be related to the soliton's velocity. McLaughlin and Scott [17] study a damped and driven sine-Gordon system modeling a Josephson junction and find a unique limiting velocity for solitons under that perturbation. The fundamental difference between their system and ours is the presence of the localized defect mode, which must be included in the reduced system.

The paper is laid out as follows. In section 2 we introduce a system of ordinary differential equations that models equation (1.1), and show the results of numerical simulations of the model. In section 3, we determine the critical velocity separating captured kinks from those that pass by the defect. In section 4, we derive formulas that are valid in a neighborhood of  $|X| = \infty$ . These are used in section 5 where we construct matched asymptotic expansions to solutions satisfying the 2-bounce resonance. We find the sequence of velocities defining the resonance windows, as well as formulas for the window widths. We also find locations of 3-bounce resonance windows and approximations for the general initial value problem. In section 6, we demonstrate the validity of this approach by comparing the formulas derived in the previous two sections with the results of numerical simulations. We summarize and include a more general discussion in section 7.

## 2 The Variational Approximation

Following Fei et al. [8], we consider a sine-Gordon model with a localized impurity at the origin, given by equation (1.1). In the absence of any impurity, i.e.  $\epsilon = 0$ , the sine-Gordon equation has the well-known family of kink solutions parameterized by velocity  $v$ :

$$u_k(x, t) = 4 \tan^{-1} \exp\left((x - vt - x_0)/\sqrt{1 - v^2}\right). \quad (2.1)$$

If we consider the system with an impurity, then solutions of small amplitude approximately satisfy the linear equation:

$$u_{tt} - u_{xx} + u = \epsilon \delta(x)u, \quad (2.2)$$

which, for  $0 < \epsilon < 2$ , has standing wave solutions

$$u_{\text{im}}(x, t) = a(t)e^{-\epsilon|x|/2},$$

where  $a(t) = a_0 \cos(\Omega t + \theta_0)$  and

$$\Omega = \sqrt{1 - \epsilon^2/4}. \quad (2.3)$$

Fei, Kivshar, and Vázquez [8] study the interaction of the kink and defect modes using a variational approximation to derive a set of equations for the evolution of the kink position  $X$ , and the defect mode amplitude  $a$ . An excellent review of the use of variational approximations in nonlinear optics is given by Malomed [16]. To derive the approximate equations, they substitute the ansatz

$$u = u_k + u_{\text{im}} = 4 \tan^{-1} \exp(x - X(t)) + a(t)e^{-\epsilon|x|/2} \quad (2.4)$$

into the Lagrangian of (1.1)

$$L = \int_{-\infty}^{\infty} \left( \frac{1}{2} u_t^2 - \frac{1}{2} u_x^2 - [1 - \epsilon \delta(x)](1 - \cos u) \right) dx. \quad (2.5)$$

Here  $X$  replaces  $x_0 + Vt$ , and  $a$  and  $X$ , the parameters characterizing the approximate solution (2.4), are regarded as unknown functions of  $t$ . It is assumed that  $a$  and  $\epsilon$  are small enough that many cross-terms can be neglected. Thus, in calculating the effective Lagrangian, all terms produced via overlap of the two modes are neglected, excepting those which include the defect potential  $\delta(x)$ . This is equivalent to assuming that the dominant means of interaction between the two modes is via the defect. Evaluating the spatial integrals of (2.5), an effective Lagrangian  $L_{\text{eff}}(X, a, \dot{X}, \dot{a})$  is obtained [8]:

$$L_{\text{eff}} = 4\dot{X}^2 + \frac{1}{\epsilon}(\dot{a}^2 - \Omega^2 a^2) - \epsilon U(X) - \epsilon a F(X), \quad (2.6)$$

where

$$\begin{aligned} U(X) &= -2 \operatorname{sech}^2(X); \\ F(X) &= -2 \tanh(X) \operatorname{sech}(X). \end{aligned}$$

The corresponding evolution equations are then given by the classical Euler-Lagrange equations for (2.6):

$$8\ddot{X} + \epsilon U'(X) + \epsilon a F'(X) = 0; \quad (2.7a)$$

$$\ddot{a} + \Omega^2 a + \frac{\epsilon^2}{2} F(X) = 0. \quad (2.7b)$$

This system has also been studied in [9]. Note that the system conserves the Hamiltonian

$$H = 4\dot{X}^2 + \frac{1}{\epsilon}(\dot{a}^2 + \Omega^2 a^2) + \epsilon U(X) + \epsilon a F(X) \quad (2.8)$$

and that as  $|X| \rightarrow \infty$ ,  $U \rightarrow 0$  and  $F \rightarrow 0$  exponentially. The energy is thus asymptotically positive definite, and must be partitioned between  $X$  and  $a$  when the soliton is far from the defect.

This system corresponds to a particle  $X$  moving in an attractive potential well  $\epsilon U(X)$  exponentially localized in a neighborhood of zero, coupled to a harmonic oscillator  $a$  by an exponentially localized term  $\epsilon a F(X)$ . Note that this model inherits many properties from the sine-Gordon system.  $U(X)$  and  $F(X)$  decay for large  $|X|$ , so that when  $|X|$  is large  $\dot{X} \approx 0$  and the kink may propagate at any constant speed, independent of the impurity mode  $a$ , which oscillates at its characteristic frequency  $\Omega$ . When  $X$  becomes small, the two equations become coupled and the kink may exchange energy with the impurity mode.

The variational method, while popular in the study of nonlinear optics, may contain significant pitfalls. First, it depends on the investigator finding an appropriate ansatz, as is done in equation (2.4). Second, even if the ansatz is chosen to be an exact representation of the initial data, there is no guarantee given by the method that the solution at a later time is well represented by an approximation of this form. Thus, one must carefully show that solutions of the full PDE system are well approximated by the ansatz.

Figure 1.1 should be compared to figure 2.1. The former plots the output versus input velocities for the full PDE, as computed in [8]. It shows a critical velocity  $v_c \approx 0.166$ , and a finite number of resonance windows of decreasing width as  $v \nearrow v_c$ . In between these resonance windows, incoming solutions are trapped. For speeds slightly above  $v_c$ , it appears that  $v_f = O((v_i - v_c)^{\frac{1}{2}})$ . The latter shows the same experiment for the ODE. This shows a critical velocity  $v_c \approx 0.17$ , in reasonable agreement with the PDE dynamics, a sequence of reflection windows, and a square-root profile just to the right of  $v_c$ . There are a few major differences between the two numerical experiments. The first is that the PDE dynamics show only a finite number of resonance windows, while the number of resonance windows for the ODE dynamics will be shown below to be infinite. Second, the regions between the resonance windows do not usually give rise to trapped solutions. It was shown in [9] that almost all solutions have nonzero  $v_{\text{out}}$ . This is because the variational ODEs are Hamiltonian, and a variant of the Poincaré recurrence theorem implies that the probability that a solution is trapped is zero. Also note, that the exit speed in the resonance windows for the PDE computation is significantly smaller than the input speed, while for the ODE, the  $v_{\text{out}} = -v_{\text{in}}$  at the center of the resonance windows. The variational ansatz (2.4) ignores energy that is lost via transfer to radiation modes. In [9], a dissipative correction to (2.7) is derived that takes this into account. This eliminates most of the sensitive dependence of  $v_{\text{out}}$  on  $v_{\text{in}}$  and replaces the chaotic regions with trapping regions. Nonetheless, we believe the Hamiltonian ODE (2.7) displays the fundamental features, if not the exact details, of the two-bounce resonance.

We now describe the structure of individual solutions to the ODE (2.7). The numerical experiments were performed with initial conditions

$$X(0) = -12; \dot{X}(0) = v_{\text{in}} > 0; a(0) = 0; \dot{a}(0) = 0.$$

For a general value of  $v_{\text{in}} < v_c$ ,  $X(t)$  comes in at constant speed, speeds up near zero, slows down as it approaches  $+\infty$ , oscillates back and forth a few times,

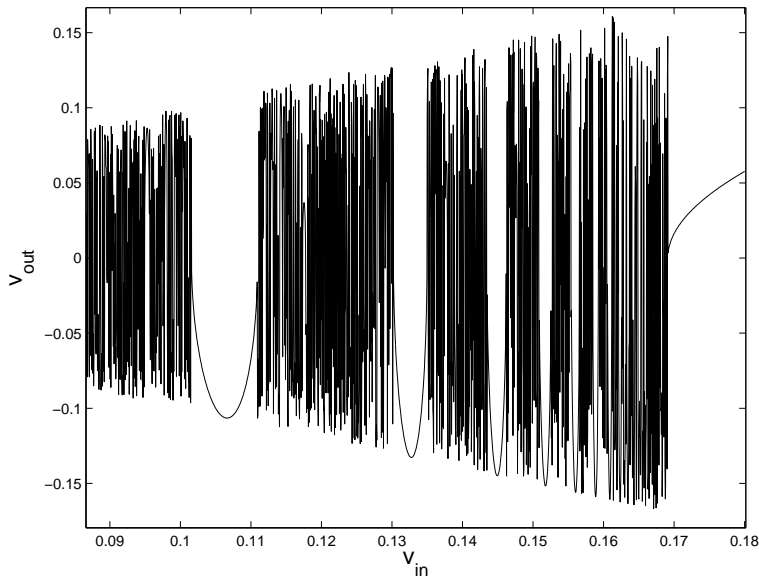


Figure 2.1: The analog of figure 1.1 for the ODE (2.7), with  $\epsilon = 0.5$ .

then emerges and heads off in either direction with finite velocity  $v_{\text{out}}$ , with  $|v_{\text{out}}| \leq v_{\text{in}}$ . The harmonic oscillator  $a(t)$ , at first grows monotonically, and then begins oscillating, interrupted by a sequence of jumps in its amplitude and phase, before settling down to a steady oscillation as  $X \rightarrow \infty$ ; see figure 2.2. This includes the  $v_{\text{in}}$  in the two-bounce resonance windows, in which the behavior is simpler:  $X(t)$  approaches plus infinity, turns around, and heads back off to minus infinity and  $a(t)$  grows, oscillates a finite number of time, and then shrinks again. At the very bottom of the resonance window (actually at a point tangent to the line  $v_{\text{out}} = -v_{\text{in}}$  in figure 2.1),  $a(t)$  actually returns all its energy to  $X(t)$ , so that  $\lim_{t \rightarrow \infty} a(t) = 0$  and  $v_{\text{out}} = -v_{\text{in}}$ . In each successive window, the  $a(t)$  undergoes one more oscillation than in the window to its left, with  $n_{\text{min}}(\epsilon)$  oscillations in the leftmost window. This number increases quickly as  $\epsilon \searrow 0$ . For example, when  $\epsilon = 0.5$ ,  $a(t)$  undergoes 4 oscillations for  $v_{\text{in}}$  in the leftmost window, 5 in the next window, etc.; see figures 2.3 and 2.4. The phrase “2-bounce resonance” was coined in [4] and refers to the fact that the kink comes in contact with the defect twice; e.g. in figure 2.3, these would be at about  $t = 80$  and  $t = 100$  when  $X = 0$ . It is during the “bounces” that the kink is in contact with the defect and exchanges energy with the defect mode. During the first interaction the soliton gives up energy to the defect mode and is trapped, and in the second, the energy is returned, and the soliton resumes propagating. We generalize this name to the 2- $n$  bounce resonance, where  $n$  denotes the number of complete oscillations of  $a(t)$ . It is possible to find in the simulations higher resonances, where the soliton interacts with the defect

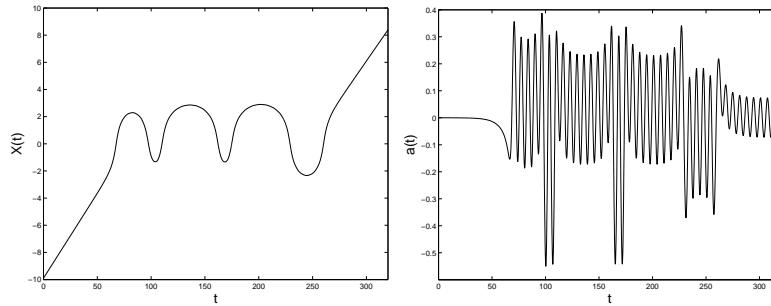


Figure 2.2:  $X(t)$  and  $a(t)$  for the numerical experiment with  $\epsilon = 0.5$  and  $v_{\text{in}} = 0.125$ .

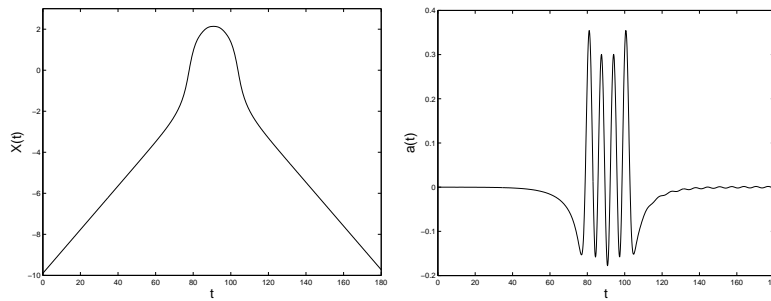


Figure 2.3:  $X(t)$  and  $a(t)$  for the numerical experiment with  $\epsilon = 0.5$  and  $v_{\text{in}} = 0.10645$ , showing the 2-4 resonance.

three or more times, before its energy is returned and it resumes propagating. These resonance windows are naturally much narrower. Interspersed between the reflection and transmission windows is a set of initial conditions of measure zero in which the solutions are chaotic and  $X(t)$  remains bounded for all time.

It is helpful to look at projections of the solutions in the  $(X, \dot{X})$  phase space. If we ignore the term  $\epsilon a F'(X)$  in (2.7a), the simplified system has an elliptic fixed point at  $(0, 0)$  and degenerate saddle-like fixed points at  $(\pm\infty, 0)$ , connected by a pair of heteroclinic orbits, which split the phase space into three regions, as is shown in figure 2.5. In region  $R_1$  (respectively  $R_3$ ), solutions move right (respectively left) along trajectories that asymptote to horizontal lines for large  $|X|$ . Solutions in region  $R_2$  oscillate clockwise, remaining bounded for all time. When the coupling to  $a(t)$  is restored, these trajectories are no longer invariant, and the solution may cross over the separatrices. A typical solution starting in region  $R_1$  will cross over the separatrix, oscillate inside  $R_2$  several times, then exit to either region  $R_1$  or  $R_3$ ; as is shown in the first graph of figure 2.6. In a 2-bounce solution,  $X(t)$  must first cross from  $R_1$  to  $R_2$ , undergo

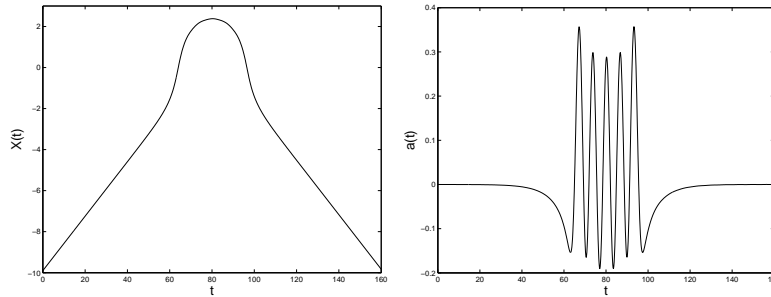


Figure 2.4:  $X(t)$  and  $a(t)$  for the numerical experiment with  $\epsilon = 0.5$  and  $v_{\text{in}} = 0.1327$ , showing the 2-5 resonance.

half an oscillation, and then cross into  $R_3$  and propagate back toward  $-\infty$ ; as is seen in the second graph of figure 2.6 for an illustration.

### 3 Determination of the critical velocity

To compute the critical velocity  $v_c$ , we will use a Melnikov computation [11, 18]. Essentially, we write down the time rate of change of the energy contained in  $X(t)$ , and integrate this over a separatrix orbit to find the total energy transferred away from  $X$  as it travels from  $-\infty$  to  $+\infty$ . Then, if the initial energy is greater than the energy loss, then  $X$  reaches  $+\infty$ . If the energy is less, than the trajectory crosses the separatrix and turns around.

We rescale the time variable  $t \rightarrow \sqrt{\frac{\epsilon}{2}}t$ . Under this scaling, the equations become:

$$4\ddot{X} + U'(X) + aF'(X) = 0; \quad (3.1a)$$

$$\ddot{a} + \lambda^2 a + \epsilon F(X) = 0 \quad (3.1b)$$

where

$$\lambda^2 = \frac{2}{\epsilon} - \frac{\epsilon}{2}.$$

This removes the explicit  $\epsilon$ -dependence from (3.1a) and fixes the leading-order time scale.

We consider the initial value problem defined by (3.1) together with the “initial condition” that as  $t \rightarrow -\infty$ ,

$$X \rightarrow -\infty; \dot{X} \rightarrow V \quad a \rightarrow 0 \quad \dot{a} \rightarrow 0. \quad (3.2)$$

Because (3.1) is autonomous, this is insufficient to specify a unique solution, and we should append the condition that as  $t \rightarrow -\infty$ ,

$$X \sim X_0 - Vt.$$

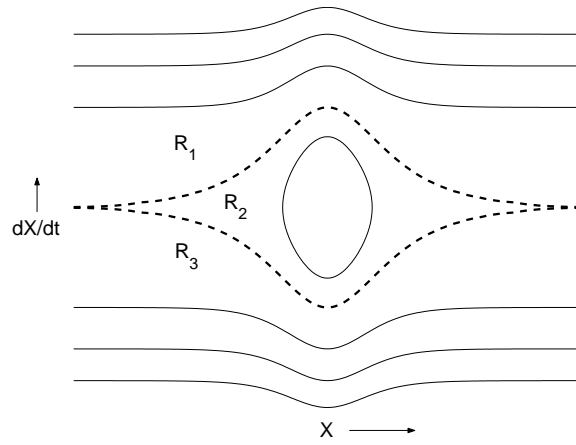


Figure 2.5: The phase plane of the uncoupled  $X$  dynamics, divided into three regions by a pair of degenerate heteroclinic orbits.

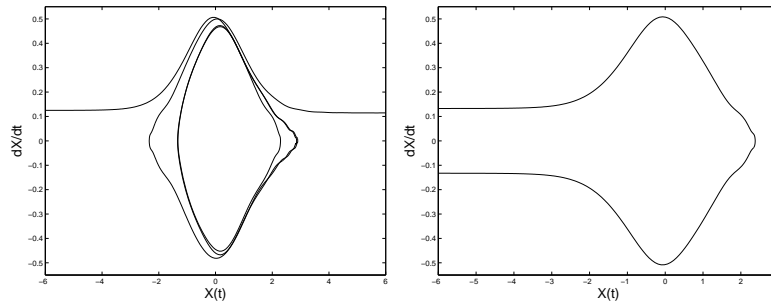


Figure 2.6: Projections into  $(X, \dot{X})$  plane of the solutions shown in figure 2.2 (left) and figure 2.4 (right).

When  $\epsilon = 0$ ,  $a = \dot{a} = 0$  defines an invariant subspace  $\mathcal{P}_0$  of (3.1) with trajectories confined to lie on surfaces along which the energy

$$E = 2\dot{X}^2 + U(X) \quad (3.3)$$

is constant.

As seen in figure 2.5, the unperturbed  $X$ -phase space features bounded periodic orbits for  $E < 0$ , unbounded orbits which tend to a finite velocity at  $|t| \rightarrow \infty$  for  $E > 0$  and separatrix orbits with  $E = 0$  along which  $\dot{X} \rightarrow 0$  as  $|X| \rightarrow \infty$ . Along this heteroclinic orbit

$$X = \pm \sinh^{-1}(t - t_1) \quad (3.4)$$

where  $t_1$  is the ‘‘symmetry time’’ of the orbit. In the calculation that follows, we will set  $t_1 = 0$  for ease of notation. We will need to include nonzero  $t_1$  later, and will reintroduce it at key locations in the computation.

When  $\epsilon > 0$ ,  $\mathcal{P}_0$  ceases to be invariant, and energy is transferred from  $X$  to  $a$ . Because the coupling term  $F(X)$  decays exponentially, almost all the energy exchange takes place when  $X$  is small. This justifies calculating the change of energy along the separatrix, because very little of the change of energy is due to the tails. We now compute the change in energy for small values of  $\epsilon$ , as  $X$  travels from  $-\infty$  to  $+\infty$ . We do this using a Melnikov integral.

Using equations (3.3) and (3.1a), the time derivative of the energy in  $E$  is

$$\begin{aligned} \frac{dE}{dt} &= (4\ddot{X} + U'(X))\dot{X} \\ &= -aF'(X)\dot{X}. \end{aligned}$$

Integrating this over the separatrix orbit yields the approximate total loss of energy of the soliton over the trajectory in the form of a Melnikov integral:

$$\begin{aligned} \Delta E &= \int_{-\infty}^{\infty} \frac{dE}{dt} dt \\ &= - \int_{-\infty}^{\infty} F'(X(t))\dot{X}(t)a(t) dt. \end{aligned}$$

Plugging the various formulae into the separatrix (3.4) (using the plus signs for right-moving trajectories and allowing  $t_1 = 0$ , which does not effect this calculation):

$$\begin{aligned} F &= -2 \operatorname{sech} X \tanh X = \frac{-2t}{1+t^2}; \\ F' &= -4 \operatorname{sech}^3 X + 2 \operatorname{sech} X = \frac{-4}{(1+t^2)^{3/2}} + \frac{2}{(1+t^2)^{1/2}}; \\ \dot{X} &= \operatorname{sech} X = (1+t^2)^{-1/2}. \end{aligned}$$

This gives the Melnikov integral

$$\Delta E = - \int_{-\infty}^{\infty} \left( \frac{-4}{(1+t^2)^2} + \frac{2}{1+t^2} \right) a(t) dt. \quad (3.5)$$

We evaluate  $\Delta E$  by first computing  $a(t)$  and then using this in equation (3.5). Using initial condition (3.2), we may solve for  $a$  by variation of parameters:

$$\begin{aligned} a &= \frac{\epsilon}{\lambda} \cos \lambda t \int_{-\infty}^t F(X(\tau)) \sin \lambda \tau d\tau - \frac{\epsilon}{\lambda} \sin \lambda t \int_{-\infty}^t F(X(\tau)) \cos \lambda \tau d\tau \\ &= -\frac{\epsilon}{\lambda} \int_{-\infty}^t F(X(\tau)) \sin \lambda(t - \tau) d\tau \\ &= \frac{2\epsilon}{\lambda} \int_{-\infty}^t \sin \lambda(t - \tau) \frac{\tau}{1 + \tau^2} d\tau. \end{aligned} \quad (3.6)$$

In fact, only the even component of  $a(t)$  will be needed to evaluate  $\Delta E$ . This is given by

$$a_e = \frac{\epsilon}{\lambda} \int_{-\infty}^{\infty} \sin \lambda(t - \tau) \frac{\tau}{1 + \tau^2} d\tau. \quad (3.7)$$

This may be evaluated by introducing the complex exponential and closing the integral in the lower half  $\tau$ -plane, which gives a contribution from the pole at  $\tau = -i$ :

$$a_e = -\frac{\epsilon \pi e^{-\lambda}}{\lambda} \cos \lambda t. \quad (3.8)$$

Then, putting (3.7) into (3.5) and using complex exponentials, gives

$$\Delta E = \frac{\pi \epsilon}{\lambda} e^{-\lambda} \int_{-\infty}^{\infty} \left( \frac{-4}{(1+t^2)^2} + \frac{2}{1+t^2} \right) e^{i\lambda t} dt. \quad (3.9)$$

This may be closed in the upper complex plane, where the residues at  $t = i$  leads to the final answer:

$$\Delta E = -2\pi^2 \epsilon e^{-2\lambda}. \quad (3.10)$$

Note that a Melnikov integral has been evaluated to determine the leading order change of energy, essentially providing the  $O(\epsilon)$  term in an infinite series expansion of this change. What was found was actually  $O(\epsilon e^{-\sqrt{\frac{2}{\epsilon}}})$ , which is significantly smaller. Alarmingly, then, the  $O(\epsilon^2)$  or subsequent terms might dwarf the first term in the expansion, rendering the Melnikov integral meaningless. A related phenomenon was studied by Holmes, Marsden, and Scheurle [14], who studied the rapidly forced pendulum

$$\theta'' + \sin \theta = \epsilon^p \sin \frac{t}{\epsilon}$$

and were able to show that for  $p \geq 8$  the Melnikov integral accurately measures the exponentially small separatrix splitting. They were subsequently able to reduce  $p$ . Delshams and Seara then removed this restriction on the size of the rapid forcing term in [5]. We therefore have confidence that the Melnikov integral correctly measures the energy change. The numerical evidence of section 6 is also shown to be in excellent agreement.

Equation (3.10) may then be used to find the critical velocity:

$$2 \left( \frac{dX}{dt} \right)^2 = |\Delta E| = 2\pi^2 \epsilon e^{-2\lambda} \quad (3.11)$$

$$V_c \equiv \frac{dX}{dt} = \pi \sqrt{\epsilon} e^{-\lambda}. \quad (3.12)$$

Recall that  $t$  has been scaled by a factor of  $\epsilon/2$ . Removing this scaling gives a critical velocity

$$v_c = \frac{\pi \epsilon}{\sqrt{2}} e^{-\lambda}. \quad (3.13)$$

We may compute output velocity  $V_{\text{out}}$  for slightly supercritical input velocity  $V_{\text{in}} = \pi \sqrt{\epsilon} e^{-\lambda} (1 + \delta_V)$  using the energy:

$$2V_{\text{in}}^2 - \Delta E = 2V_{\text{out}}^2$$

so that

$$V_{\text{out}} \sim \sqrt{2\delta_V} V_c.$$

This gives the characteristic square root behavior of the curve in figure 2.1 to the right of  $v_c$ .

We briefly mention two generalizations of the above Melnikov analysis that will be exceptionally useful in later sections. On the first near-heteroclinic orbit, we assume that no energy resides in  $a(t)$ . On subsequent near-heteroclines,  $a(t)$  is actively oscillating, so we first suppose that as  $t \rightarrow -\infty$ ,

$$a(t) \sim \frac{2\epsilon\pi e^{-\lambda}}{\lambda} A \cos \lambda(t - T), \quad (3.14)$$

where  $A$  and  $T$  will be determined later. Then, since equation (3.1b) is linear, the contribution due to this term merely adds to the contribution already calculated. As before, only the even part of  $a(t)$  is needed for the calculation. Thus using  $\cos \lambda(t - T) = \cos \lambda T \cos \lambda t + \sin \lambda T \sin \lambda t$ , the total change of energy is thus

$$\Delta E = (4A \cos \lambda T - 2)\pi^2 \epsilon e^{-2\lambda}. \quad (3.15)$$

Depending on the magnitude and sign of  $A \cos \lambda T$  the energy change may be positive or negative

Second, we consider the Melnikov integral computed along the separatrix in the lower half-plane. System (2.7) obeys the symmetry

$$(X, \dot{X}, a, \dot{a}; t) \rightarrow (-X, -\dot{X}, -a, -\dot{a}; t),$$

so that the Melnikov integral can be computed directly. Assuming the limiting behavior (3.14), the change of energy is

$$\Delta E = (-4A \cos \lambda T - 2)\pi^2 \epsilon e^{-2\lambda}. \quad (3.16)$$

### 3.1 The full expansion of $a(t)$

In later sections, we will need more detailed knowledge of the form of  $a(t)$ . By equations (3.6)-(3.8),

$$a = 2a_e - \frac{2\epsilon}{\lambda} \int_t^\infty \sin \lambda(t - \tau) \frac{\tau}{1 + \tau^2} d\tau.$$

We obtain the asymptotic expression as  $t \rightarrow +\infty$  by integrating by parts to obtain

$$a(t) \sim \frac{2\epsilon}{\lambda^2} \left( \frac{t - t_1}{(t - t_1)^2 + 1} + O(\lambda^{-2}) \right) - \frac{2\epsilon\pi e^{-\lambda}}{\lambda} \cos \lambda(t - t_1). \quad (3.17)$$

Similarly, as  $t \rightarrow -\infty$ ,

$$a(t) \sim \frac{2\epsilon}{\lambda^2} \left( \frac{t - t_1}{(t - t_1)^2 + 1} + O(\lambda^{-2}) \right) \quad (3.18)$$

with no exponentially small oscillatory term. Here we have re-introduced the dependence of the solution on the symmetry time  $t_1$  from (3.4), ignored during the calculation above for transparency of notation. The algebraically small terms decay for large  $t$ , so as  $t \rightarrow \infty$ , it is the exponentially small oscillating term that dominates. However, when we use the method of matched asymptotic expansions, we will assume that  $t$  is exponentially large of the appropriate size so that the leading order algebraic term and the oscillation are of the same size.

## 4 Solutions near $|X| = \infty$

In the next two sections we construct matched asymptotic solutions to (3.1) by matching near-separatrix solutions to solutions valid near  $|X| = \infty$ . The solution for large  $|X|$  may be expanded as a near-saddle approach to the degenerate saddle points at infinity. Nearly heteroclinic orbits alternate with near-saddle approaches. Near-saddle expansions for linear saddle points are common. In that case, exponential growth of solutions away from the saddle point matches to exponential decay of homoclinic orbits. Finite nonlinear saddle points corresponding to bifurcations for Hamiltonian systems have been analyzed by Diminnie and Haberman [6, 7] and Haberman [12, 13]. In the current work, the nonlinear saddle is at infinity, and we do not believe that such an expansion has been analyzed before. In the present case, solutions in the near-saddle region have finite-time singularities which match to the logarithmic growth of the heteroclinic orbits. We note from the conservative system (3.1) and expansion (3.17)

that the contribution due to  $aF'(X)$  is exponentially small for large  $t$ , so that to leading order

$$4\ddot{X} + U'(X) = 0 \quad (4.1)$$

with the energy given by (3.3).  $U(X)$  may be approximated in a neighborhood of  $\pm\infty$  by

$$U \sim -8e^{\mp 2X}.$$

We may then form approximations valid for large  $X$  in two different ways depending on whether the energy  $E$  is positive or negative. Phase portraits of (4.1), shown in figure 2.5, may clarify the results that follow.

If  $E = 2V^2 > 0$ , then the solution of (4.1) corresponding to the near-saddle approach is given by

$$e^{\pm X} = \pm \frac{2}{V} \sinh V(t - t_*) \text{ as } X \rightarrow \pm\infty. \quad (4.2)$$

The  $\pm$  sign on the left side of the equation determines whether  $X \rightarrow \pm\infty$ , and the sign on the right must be chosen so that  $\pm(t - t_*)$  is positive. The constant  $t_*$  is the finite blowup time at which time the near-saddle approach goes to infinity. The  $V$  in the notation is used intentionally, as it gives the asymptotic velocity of the near approach to the saddle.

The solution for the near-saddle approach with  $E = -2M^2 < 0$  is given by

$$e^{\pm X} = \frac{2}{M} \cos M(t - t_{**}) \quad (4.3)$$

which has finite time singularities forward and backward in time when  $M(t - t_{**}) = \pm\frac{\pi}{2}$  and is symmetric about the symmetry time  $t = t_{**}$ .

For large  $|X|$ ,  $F(X) \sim \mp 4e^{\pm X}$ , so that from (3.1b),

$$\ddot{a} + \lambda^2 a \sim \pm 4\epsilon e^{\pm X}.$$

Since  $\lambda \gg 1$ , the asymptotic expansion of  $a(t)$  is given by

$$a \sim \pm \frac{4\epsilon}{\lambda^2} e^{\pm X(t)} + c_1 \cos \lambda(t - t_1) + c_2 \sin \lambda(t - t_1), \quad (4.4)$$

where (4.2) or (4.3) may be used depending on the circumstance. Equation (4.4) shows that near the saddle approaches  $a(t)$  consists of simple harmonic oscillations about a slowly varying mean (which increases in forward and backwards time toward the finite time singularities), all of which can clearly be seen in the numerical calculations. The saddle approach with  $E < 0$ , described in detail in the next section must match backwards in time to (3.17), so that  $c_2 = 0$  and  $c_1 = -\frac{2\epsilon\pi e^{-\lambda}}{\lambda}$ . Matching this near-saddle approach for  $a(t)$  forward in time shows how this exponentially small oscillation is added as previously stated in (3.14).

## 5 Construction of solutions near the separatrix

We now construct an approximation to the initial value problem for the scaled model equation (3.1) under the assumption that the initial velocity is subcritical. To be precise, we consider the “initial value problem” defined by (3.1) and (3.2). We let  $V$  refer to the limiting velocity in the scaled model, and reserve  $v$  for the velocity in the physical variables. We assume that  $V > 0$  is less than the critical value found in (3.12). Then, we may make the assumption that  $E(t)$  stays exponentially close to 0, its value along the heteroclinic orbit.  $X(t)$  may then be approximated in two different ways, depending on whether  $X$  is near a heteroclinic orbit or  $X$  is close to infinity. These two approximations may then be connected by their limiting behaviors to give a matched asymptotic expansion. When  $X$  may be approximated by a heteroclinic orbit

$$X \approx \pm \sinh^{-1}(t - t_j),$$

where  $t_j$  is the “symmetry time” at which  $X = 0$  for the  $j$ th nearly heteroclinic orbit. For  $|X|$  large, the solution is given by formulas (4.2) and (4.3). The exponentially small part of  $a(t)$  contributes to the analysis, as it determines the energy difference between subsequent approaches to infinity.

### 5.1 2-bounce solutions

The 2-bounce solution can be constructed from the following pieces:

1. A near saddle approach to  $X = -\infty$  with energy  $E_0 = 2V_0^2$ :

$$e^{-X} = -\frac{2}{V_0} \sinh V_0(t - t_*), \quad (5.1a)$$

with  $V_0 < V_c$  as given by (3.12).

2. a heteroclinic orbit with  $dX/dt > 0$ :

$$\sinh X = t - t_1, \quad (5.1b)$$

3. a near saddle approach to  $X = +\infty$  with negative energy  $E = -2M_1^2$ :

$$e^X = \frac{2}{M_1} \cos M_1(t - t_{**}), \quad (5.1c)$$

4. a heteroclinic orbit with  $dX/dt < 0$ :

$$\sinh X = -(t - t_2), \quad (5.1d)$$

5. and a near saddle approach to  $X = -\infty$  with positive energy  $E = 2V_2^2$ :

$$e^{-X} = \frac{2}{V_2} \sinh V_2(t - t_{***}). \quad (5.1e)$$

The solution can be summarized as a succession of near-saddle approaches, connected by heteroclinic orbits. Since the change of energy between consecutive near-saddle approaches is given by (3.10), we see

$$-2M_1^2 - 2V_0^2 = -2\pi^2\epsilon e^{-2\lambda}. \quad (5.2)$$

We now need to compute the change of energy along the second heteroclinic connection. We must first compute the symmetry time  $t_2$  of the second heteroclinic orbit, which is done via leading order matching of  $X(t)$ . The algebraically small components of  $a(t)$  can be obtained from  $X(t)$  by regular perturbation, and thus match immediately once  $X$  satisfies matching conditions. The separatrix is given by  $X = -\sinh^{-1}(t - t_j)$ , and the oscillatory part of  $a(t)$  is given by  $-\frac{2\epsilon\pi e^{-\lambda}}{\lambda} \cos \lambda(t - t_1)$  in backwards time. Shifting time by  $t_2$ , we arrive at the energy change computed in (3.16) with  $A = -1$  and  $T = t_2 - t_1$ . The analytic criterion for a 2-bounce solution is that the energy be positive after the second heteroclinic transition, i. e.

$$E_2 = 2V_0^2 - 2\pi^2\epsilon e^{-2\lambda} + (4 \cos \lambda(t_2 - t_1) - 2)\pi^2\epsilon e^{-2\lambda} > 0. \quad (5.3)$$

If  $E_2 < 0$ , then the energy at this saddle approach is less than zero, and the solution does not escape at this saddle approach.

The large time singularity of the first heteroclinic orbit (5.1b):

$$e^{-X} \sim \frac{1}{2} \frac{1}{(t - t_1)}$$

must match the singularity of (5.1c) as  $M_1(t - t_{**}) \searrow -\pi/2$ :

$$e^{-X} \sim \frac{M_1}{2} \frac{1}{M_1(t - t_{**}) + \frac{\pi}{2}},$$

yielding

$$t_{**} - t_1 = \frac{\pi}{2M_1}.$$

A similar calculation yields

$$t_2 - t_{**} = \frac{\pi}{2M_1}.$$

Combining these gives

$$t_2 - t_1 = \frac{\pi}{M_1}. \quad (5.4)$$

Note that this is exactly half the period of a closed orbit with  $E = -2M_1^2$ . Matching (5.1a) to (5.1b) yields  $t_* = t_1$ , and matching (5.1d) to (5.1e) yields  $t_{***} = t_2$ .

## 5.2 The 2-bounce resonance and the width of the 2-bounce window

This does not suffice to determine resonant values of  $V_0$ , because we still need to satisfy the condition that the oscillatory component of  $a(t)$  vanishes in component 5 of the solution. Thus, at this stage we require a matching condition on the exponentially small oscillating part of  $a(t)$ . Two-bounce resonant solutions are defined by the condition that  $E_2 = 2V_0^2$ . From (5.3), this requires that  $\cos \lambda(t_2 - t_1) = 1$ . Using (5.4), we obtain the analytic condition for 2-bounce resonant solutions that

$$\frac{\lambda\pi}{M_1} = 2\pi n,$$

where  $n > 0$  is an integer, so that  $\Delta E = 2\pi^2\epsilon e^{-2\lambda}$ . Thus, the second jump in energy exactly cancels the first, and all of the energy is returned to the propagating mode  $X$ . This gives a quantization condition

$$M_1 = \frac{\lambda}{2n}. \quad (5.5)$$

We can combine this with equation (5.2), to obtain a formula for the initial velocity of the 2- $n$  resonant solution

$$V_n = \sqrt{\pi^2\epsilon e^{-2\lambda} - \frac{\lambda^2}{4n^2}}. \quad (5.6)$$

$V_n$  denotes the (scaled) initial velocity of the soliton in 2- $n$  resonance with the defect mode. In order that for  $V_n$  to be well-defined,  $n$  must satisfy

$$n \geq n_{\min}(\epsilon) \equiv \frac{\lambda e^\lambda}{2\pi\sqrt{\epsilon}}. \quad (5.7)$$

This gives a lower bound on the number of  $a$ -oscillations in a 2 bounce resonance, and explains why the observed resonance windows disappear as  $\epsilon$  is increased.

We may find the width of the 2- $n$  resonance window as follows. If the energy change along the second heteroclinic orbit satisfies  $\Delta E > 2M_1^2$ , then the solution has positive energy, the trajectory crosses the separatrix, and the soliton escapes. If  $\Delta E < 2M_1^2$ , then the solution remains bounded, and will approach minus infinity before turning around another time. Therefore, the boundaries of the 2- $n$  window, as a function of  $M_1$  are given by the values of  $M_1$  where

$$\Delta E = 2M_1^2$$

in (5.3), i.e. if

$$\cos \frac{\lambda\pi}{M_1} = \frac{1}{2} \left( 1 + \frac{M_1^2}{\pi^2\epsilon e^{-2\lambda}} \right).$$

Letting  $M_1 = \frac{\lambda}{2(n+\delta)}$ , then

$$\cos 2\pi(n + \delta) = \cos 2\pi\delta = \frac{1}{2} \left( 1 + \frac{n_{\min}^2(\epsilon)}{(n + \delta)^2} \right). \quad (5.8)$$

Considering first the width of the leftmost window, we let  $n = \text{int}(n_{\min}(\epsilon)) + 1$ , then  $\delta^2 = \frac{1}{2n\pi^2}(1 - \text{fr}(n_{\min}(\epsilon)))$ , where  $\text{int}(Z)$  and  $\text{fr}(Z)$  are the integer and fractional parts of  $Z$ . Restricting our attention to the smaller windows closer to  $v_c$ , if  $n \gg n_{\min}(\epsilon)$ , then  $\cos 2\pi\delta \approx \frac{1}{2}$ , or  $\delta \approx \pm \frac{1}{6}$ . The left and right edges of the  $n$ th resonance window have velocity approximately

$$V_{n\pm} = \sqrt{\pi^2 \epsilon e^{-2\lambda} - \frac{\lambda^2}{4(n \pm \frac{1}{6})^2}}. \quad (5.9)$$

If  $n$  is sufficiently large, then  $\delta_n = \frac{\lambda e^\lambda}{2\pi n \sqrt{\epsilon}} \ll 1$ , and we find that the width of the  $2-n$  window is given by

$$W_n = V_{n+} - V_{n-} \approx V_c \delta_n^2 \cdot \frac{3}{n}$$

which scales as  $n^{-3}$  for large  $n$ .

### 5.3 The general initial value problem

If the second jump in energy, given by the second Melnikov calculation (5.3), is less than  $2M_1^2$ , then the soliton does not escape on the second interaction with the defect. Instead it jumps to a new energy level inside the separatrix. We can then replace the sequence (5.1) with a finite number of nearly heteroclinic orbits separated by near saddle approaches (with negative energy) in which the solution usually escapes at the last saddle approach with positive energy:

1. A near saddle approach to  $X = -\infty$ , with energy  $E_0 = 2V_0^2$ :

$$e^{-X} = -\frac{2}{V_0} \sinh V_0(t - t_*) \quad (5.10a)$$

2. A heteroclinic orbit with  $\dot{X} > 0$ , over which the change of energy is  $\Delta E_1$ , given by the Melnikov integral (3.10):

$$\sinh X = t - t_1 \quad (5.10b)$$

3. A near saddle approach alternating between  $X = \pm\infty$ , with energy  $E_j = E_{j-1} + \Delta E_j = -2M_j^2$ .

$$e^X = \frac{2}{M_j} \cos M_j(t - t_*^j) \quad (5.10c)$$

4. A heteroclinic orbit (alternating between  $\dot{X} < 0$  and  $\dot{X} > 0$ ):

$$\sinh X = \pm(t - t_j) \quad (5.10d)$$

After each nearly heteroclinic orbit, the energy is  $E_{j+1} = E_j + \Delta E_j$ . If  $E_{j+1} < 0$ , the solution has a near saddle approach with negative energy and hence returns to step 3. However, if  $E_{j+1} > 0$ , the solution escapes, and this last saddle approach is instead mathematically described by step 5.

5. If the solution escapes (at velocity  $\pm V_f$ ), then the near saddle approach at  $x = \pm\infty$  satisfies:

$$e^{\pm X} = \frac{2}{V_f} \sinh V_f(t - t_{***}) \quad (5.10e)$$

Usually the solution will escape after a finite number of bounces. However, for a set of initial velocities of zero measure, the solution will consist of an infinite number of nearly heteroclinic orbits, will not escape, and will be chaotic. The interesting dynamics take place at step 3 above. We must again consider the oscillatory part of  $a(t)$ . In analogy with expansion (3.17), after  $j$  near-heteroclinic orbits,  $a(t)$  may be written

$$a(t) \sim \text{algebraically small terms} + \frac{2\epsilon\pi e^{-\lambda}}{\lambda} \sum_{k=1}^j (-1)^{k+1} \cos \lambda(t - t_k) \quad (5.11)$$

where we find  $t_k - t_{k-1} = \frac{p_i}{M_{k-1}}$ , the appropriate generalization of (5.4). The change in energy along the  $k$ th heteroclinic orbit is given by a generalization of equations (3.15)–(3.16) to include multiple oscillating terms. If the solution contains exactly  $m$  heteroclinic connections, then the change of energy over all of the connections is given by the sum of the contributions over all the  $m$  nearly heteroclinic orbits, which, after some algebraic manipulation, is

$$\Delta E_{\text{total}} = \frac{2\epsilon\pi e^{-\lambda}}{\lambda} \sum_{i=1}^m \sum_{j=1}^m (-1)^{i+j+1} \cos \lambda(t_j - t_i). \quad (5.12)$$

The condition for an  $m$ -bounce resonance is thus that  $\Delta E = 0$ , which will happen only for a measure zero set of initial velocities  $V_0$ . If this is the case, then  $X(t)$  will have interacted with the defect a total of  $m$  times. Between each pair of bounces,  $a(t)$  will have undergone an integer number of complete oscillations (plus a small phase shift). We may thus construct, in a manner similar to that above, the  $m$ -( $q_1, q_2, \dots, q_{m-1}$ ) bounce window. Of course many of windows do not contain a complete resonance, i.e. there does not exist a velocity in the window for which all energy is returned to the propagating mode. When all the windows of initial conditions that eventually escape to  $\pm\infty$  are removed, what remains is a Cantor-like set of initial conditions that are trapped for all positive time.

## 5.4 The 3-bounce resonance

It is also possible to construct the three-bounce resonance solutions, which look in phase space like figure 5.1. Note that our matched asymptotic expansion depends on  $|X| \gg 1$ , but this figure shows that  $X \approx 2$  is sufficient. Although such resonance windows are too narrow to see with the naked eye in figure 2.1, careful examination of the data, and use of symmetries allows us to discover the three-bounce resonance windows. Note that the two-bounce solutions consist of

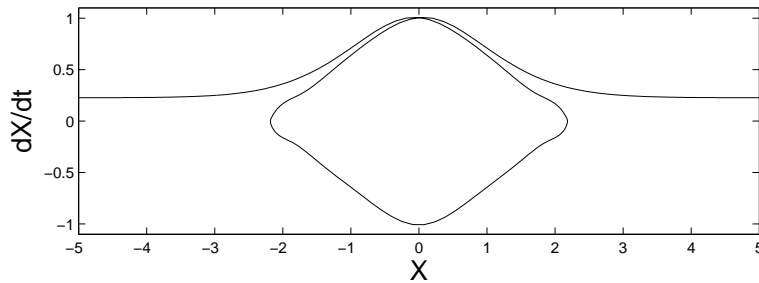


Figure 5.1: A phase-plane portrait of a 3-bounce resonant solution of equation (3.1).

$X$  and  $a$  which are even functions of  $t$  (with the time origin shifted to be the midpoint between the two singularity times). Similarly (3.1) admits solutions in which both  $X(t)$  and  $a(t)$  are odd. A three bounce resonant solution is an odd function of time, in which there are three energy jumps and  $a(t) \rightarrow 0$  as  $|t| \rightarrow \infty$ . We may assume that the three singularity times are  $-t_0$ ,  $0$ , and  $t_0$ . Then we note that for the solution to be odd, the energy level  $E_1$  for  $t \in (-t_0, 0)$  must be the same as the energy level  $E_2$  for  $t \in (0, t_0)$ , so  $\Delta E = 0$  along the second heteroclinic orbit, i.e.

$$\Delta E = (4 \cos \lambda t_0 - 2)\pi^2 \epsilon e^{-2\lambda} = 0. \quad (5.13)$$

Therefore  $\cos \lambda t_0 = \frac{1}{2}$  or

$$\lambda t_0 = 2n\pi \pm \frac{\pi}{3}.$$

By our standard reasoning this gives

$$V = \sqrt{\pi^2 \epsilon e^{-2\lambda} - \frac{\lambda^2}{4(n \pm \frac{1}{6})^2}}$$

which is exactly the formula we obtained in (5.9) when we ignored a small term in that calculation. Therefore very close to the edge of each 2-bounce window, on either side, there exists a symmetric 3-bounce window. We may check that if before the second energy jump

$$a(t) \sim -2 \cos\left(\lambda t \pm \frac{\pi}{3}\right),$$

then afterward

$$a(t) \sim 2 \cos\left(\lambda t \mp \frac{\pi}{3}\right)$$

so the solution is odd, and we don't need to compute the third interaction. In figure 5.2, we show the  $a(t)$  for the two 3-bounce windows to the immediate left and right of the first 2-bounce window shown in figure 2.1. Asymmetric 3-bounce windows also exist, in which  $a$  oscillates a different number of times on the first approach to infinity than it does on the second.

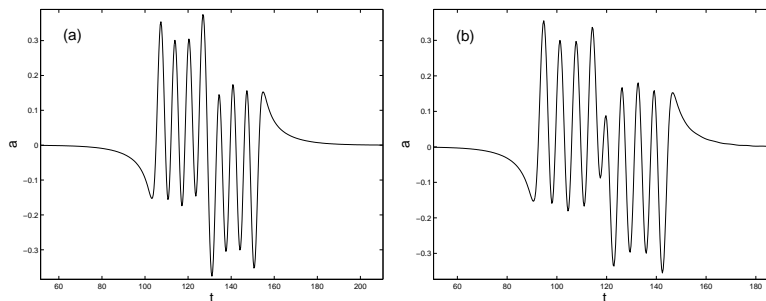


Figure 5.2: The two 3-bounce resonant solutions ( $a(t)$  only) to the left and right of the first 2-bounce window in figure 2.1. In (a),  $v=0.09796$ . In (b),  $v = 0.11301$ .

## 6 Numerical verification

The analysis of the previous section has given us formulas by which we may compute several features of the solution, as a function of the defect strength  $\epsilon$ . These include, the critical velocity  $v_c$ , the number of oscillations contained in the solution in the leftmost resonance window ( $n_{\min}(\epsilon)$ ), and the locations of the 2-bounce resonance windows, as well as their widths.

### Critical velocities

Figure 6.1, shows the numerically computed critical velocities for the values  $\epsilon \in \{\frac{1}{8}, \frac{1}{4}, \frac{1}{2}, 1\}$ , as well as  $v_c = \pi\epsilon \exp -\lambda/\sqrt{2}$ . Of course, both the curve of calculated velocities, as well as the numerically computed velocities approach zero as  $\epsilon \rightarrow 0$ , so we must show they approach zero at the same rate to validate our theory. The lower half of the figure shows the ratio of the numerical and asymptotic values, which are correct to within 6% for  $\epsilon = 1$  and to within 0.2% for  $\epsilon = 1/8$ .

### Predicted minimum $a$ -oscillations for resonance ( $n_{\min}(\epsilon)$ )

For the values  $\epsilon = \{\frac{1}{4}, \frac{1}{2}, 1\}$ , formula (5.7) yields  $n_{\min}(\epsilon)$  (rounded up to the nearest whole number:  $n_{\min}(\frac{1}{4}) = 15$ ,  $n_{\min}(\frac{1}{2}) = 4$ , and  $n_{\min}(1) = 1$ , which are precisely the values found via numerical experiment. The formula gives  $n_{\min}(\frac{1}{8}) = 98$ . The fewest oscillations seen in the numerical experiments with  $\epsilon = \frac{1}{8}$  was 100, but the equations are very stiff when  $\epsilon$  and  $v_{\text{in}}$  are very small, and smaller values of  $v_{\text{in}}$  were not investigated.

### Resonance windows

The comparison of  $v_N$  with numerically computed values is shown in Figures 6.2 for  $\epsilon = 1/4$ . Many of the resonance windows are well-predicted. We may gain

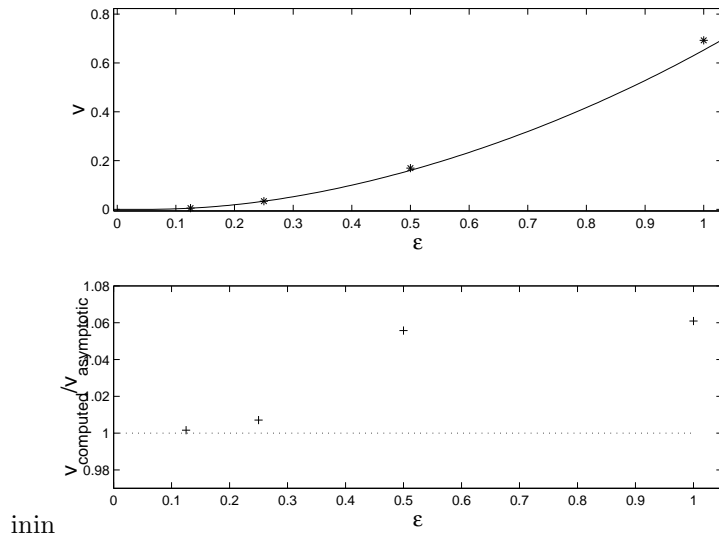


Figure 6.1: (Top) Critical velocity as a function of velocity, numerical +, and via asymptotic calculation (solid line). (Bottom) Ratio of numerical to asymptotic calculated values.

more insight by considering equation (5.6) as defining  $n$  as a function of  $V$  (and hence as a function of the unscaled velocity  $v$ ). In figure 6.3 we plot  $\cos 2\pi n(v)$  as a function of  $v$ . If  $n \in \mathbb{Z}$ , then  $\cos 2\pi n = 1$ . Therefore the 2-bounce resonance window centers (i. e. the resonant initial velocities) are given by the points where the curve  $y = \cos 2\pi n(v)$  is tangent to the line  $y = 1$ . Equation (5.8) (with  $n + \delta$  replaced by  $n(v)$ ) gives the edges of the resonance windows. Therefore to the immediate left and right of the resonance window centers, the curve  $y = \cos 2\pi n(v)$  crosses the curve  $y = \frac{1}{2} \left( 1 + \frac{n_{\text{min}}^2(\epsilon)}{n(v)^2} \right)$ , giving the window edges. We note from the figure that this implies that the leftmost resonance windows should be narrowed with respect to the space between windows. This is confirmed in the plot of  $v_{\text{out}}$  vs.  $v_{\text{in}}$ . Finally, the reasoning of section 5.4 shows that the center of the 3-bounce windows should be given by the intersection of the curve  $y = \cos 2\pi n(v)$  with the line  $y = 1/2$ .

## 7 Conclusions

We have shown how a resonant exchange of energy between a soliton and defect mode gives rise to two bounce resonance windows. This was known to Campbell et al. as well as to Fei et al. However by applying perturbation techniques to a variational model of the system, we have been able to quantify this effect without recourse to statistical data fitting. The study of Fei, Kivshar, and

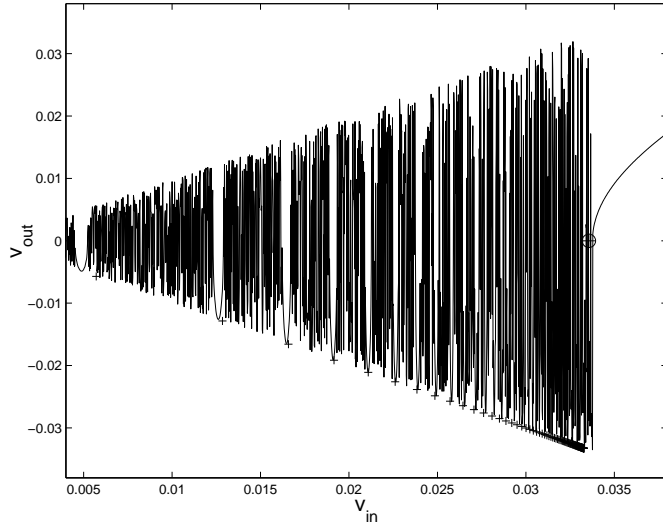


Figure 6.2: Input vs. output velocities for  $\epsilon = 1/4$  showing the predicted resonant initial velocities  $+$  and the critical velocity  $\circ$ .

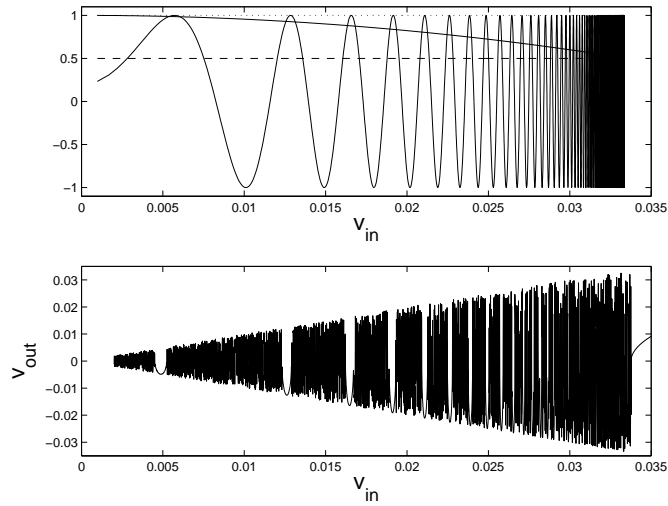


Figure 6.3: (Upper) The oscillatory curve is  $y = \cos 2\pi n(v_{\text{in}})$  as a function of  $v_{\text{in}}$ . Its intersections with the line  $y = 1$  (dotted) give the location of the 2-bounce resonant initial velocities. Intersections with the curve  $y = \frac{1}{2} \left(1 + \frac{n_{\text{min}}^2(\epsilon)}{n(v)^2}\right)$  (solid) give the edges of the resonance windows. Intersections with  $y = 1/2$  (dashed) give the 3-bounce resonant window velocities. (Lower) The curve  $v_{\text{out}}$  vs.  $v_{\text{in}}$ .

Vázquez shows remarkable fits between the numerically determined locations of the resonance windows, and also gives an implicit equation for the critical velocity that is asymptotically equivalent to our equation (3.13). The chief advantage of our method is that we are able to determine the dependence of all these quantities on  $\epsilon$  explicitly.

One of us has previously studied the model (2.7) in [9]. In that paper, an artificial coupling parameter  $\mu$  is added to (2.7). For small values of  $\mu$ , we were able to show the dynamics contained a Smale horseshoe. In that construction, capture was identified with transfer of phase space between the regions of figure 2.5 via turnstile lobes in a certain Poincaré map. That Poincaré map was ill-defined as  $\mu \rightarrow 1$ , so the results were not directly applicable to equation (2.7), although were very suggestive of the dynamics. It does indicate how the dynamics in the regions between the resonance windows in figure 2.1 depends sensitively on the input velocity. Combining this with the quantitative information contained in the current study gives a rather complete picture of the dynamics.

Other studies of the 2-bounce resonant phenomenon have often derived a formula for the resonance windows of the form

$$(v_c - v_n)^{-\frac{1}{2}} \sim nT + \theta_0$$

where  $T$  is the period of the fast oscillations, and  $\theta_0$  is some offset time. The equivalent statement in this study is given in equation (5.5). This is equivalent to setting  $\theta_0$  to zero. To attain  $\theta_0$  we would need to find further terms in (5.4), the equation for the time between interactions, in terms of the small energy-derived term  $M$ . The leading order term is  $O(M^{-1})$  and symmetries of equation (4.1) show that the  $O(1)$  term must be zero. The next term in the series is necessarily  $O(M)$ .

Many similar systems have shown the 2-bounce resonance, and the methods developed here should be adaptable to such systems. However the current system is the simplest to study for several reasons. First, it depends explicitly on a small coupling parameter  $\epsilon$ , and when  $\epsilon \rightarrow 0$  decouples into two independent oscillations. Anninos et al. derive a variational model of the kink-antikink scattering in the  $\phi^4$  experiments of Campbell et al. [1, 4]. This model does not depend explicitly on a small parameter, so an artificial one might need to be introduced. Since our formula for  $v_c$  is correct to within 6% even with  $\epsilon = 1$ , this may be a reasonable step to take. Other models do not decouple so cleanly as (3.1) as  $\epsilon \rightarrow 0$ . Nonetheless, in many systems it is possible to draw a diagram similar to figure (2.1), so we believe that a similar mechanism is at work.

## Acknowledgements

We would like to thank Phil Holmes, Michael Weinstein, Greg Kriegsmann, and Chris Raymond for helpful discussions. RG was supported by NSF DMS-0204881 and by an SBR grant from NJIT.

## References

- [1] P. Aninos, S. Oliveira, and R. A. Matzner, *Fractal structure in the scalar  $\lambda(\phi^2 - 1)^2$  model*, Phys. Rev. D **44** (1991), 1147–1160.
- [2] D. K. Campbell and M. Peyrard, *Kink-antikink interactions in the double sine-Gordon equation*, Physica D **19** (1986), 165–205.
- [3] ———, *Solitary wave collisions revisited*, Physica D **18** (1986), 47–53.
- [4] D. K. Campbell, J. S. Schonfeld, and C. A. Wingate, *Resonance structure in kink-antikink interactions in  $\phi^4$  theory*, Physica D **9** (1983), 1–32.
- [5] A. Delshams and T. M. Seara, *An asymptotic expression for the splitting of separatrices of the rapidly forced pendulum*, Comm. Math. Phys. **150** (1992), 433–463.
- [6] D. C. Diminnie and R. Haberman, *Slow passage through a saddle-center bifurcation*, J. Nonlinear Sci. **10** (2000), 197–221.
- [7] ———, *Slow passage through homoclinic orbits for the unfolding of a saddle-center bifurcation and the change in the adiabatic invariant*, Phys. D **162** (2002), 34–52.
- [8] Z. Fei, Y. S. Kivshar, and L. Vázquez, *Resonant kink-impurity interactions in the sine-Gordon model*, Phys. Rev. A **45** (1992), 6019–6030.
- [9] R. H. Goodman, P.J. Holmes, and M.I. Weinstein, *Interaction of sine-Gordon kinks with defects: phase space transport in a two-mode model*, Phys. D **161** (2002), 21–44.
- [10] R. H. Goodman, R. E. Slusher, and M. I. Weinstein, *Stopping light on a defect*, J. Opt. Soc. Am. B **19** (2002), 1635–1632.
- [11] J. Guckenheimer and P. Holmes, *Nonlinear oscillations, dynamical systems, and bifurcations of vector fields*, Springer-Verlag, New York, 1983.
- [12] R. Haberman, *Slow passage through a transcritical bifurcation for Hamiltonian systems and the change in action due to a nonhyperbolic homoclinic orbit*, Chaos **10** (2000), 641–648.
- [13] ———, *Slow passage through the nonhyperbolic homoclinic orbit associated with a subcritical pitchfork bifurcation for Hamiltonian systems and the change in action*, SIAM J. Appl. Math. **62** (2001), 488–513.
- [14] P. Holmes, J. Marsden, and J. Scheurle, *Exponentially small splittings of separatrices with applications to KAM theory and degenerate bifurcations*, Hamiltonian dynamical systems (Boulder, CO, 1987), Contemp. Math., vol. 81, Amer. Math. Soc., Providence, RI, 1988, pp. 213–244.

- [15] M. D. Kruskal and H. Segur, *Asymptotics beyond all orders in a model of crystal growth*, Stud. Appl. Math. **85** (1991), 129–181.
- [16] B. A. Malomed, *Variational methods in nonlinear fiber optics and related fields*, Progress in Optics **43** (2002), 71–193.
- [17] D. W. McLaughlin and A. C. Scott, *Perturbation analysis of fluxon dynamics*, Phys. Rev. A **18** (1978), 1652–1680.
- [18] V. K. Melnikov, *On the stability of the center for time periodic perturbations*, Trans. Moscow Math. Soc. **12** (1963), 1–57.
- [19] M. Peyrard and D. K. Campbell, *Kink-antikink interactions in a modified sine-Gordon model*, Physica D **9** (1983), 33–51.
- [20] A. Scott, *Nonlinear science*, Oxford Applied and Engineering Mathematics, vol. 1, Oxford University Press, Oxford, 1999, Emergence and dynamics of coherent structures, With contributions by Mads Peter Sørensen and Peter Leth Christiansen.
- [21] Y. Tan and J. Yang, *Complexity and regularity of vector-soliton collisions*, Phys. Rev. E **64** (2001), 056616.